CARACTERÍSTICAS AERODINÁMICAS DE UN AVIÓN NO TRIPULADO POR MEDIO DE ENSAYOS DE TÚNEL DE VIENTO Y ANÁLISIS NUMÉRICO

PEDRO J. BOSCHETTI [1], ELSA M. CÁRDENAS [1], GABRIELA QUIJADA [2], GAUDIS VERA [2], LUIS MUJICA [2], Y PEDRO J. GONZÁLEZ [1]

[1] Universidad Simón Bolívar, Departamento de Tecnología Industrial.
e-mail: pboschetti@usb.ve / elsacardenas@usb.ve / pedrogonzalez@usb.ve
[2] Universidad Simón Bolívar, Postgrado en Ingeniaría Mecánica. e-mail: gmquijadam@gmail.com / gaudis9anghi@gmail.com / mujicarluis@gmail.com

Recibido: abril 2015 Aprobado para publicación: diciembre 2015

RESUMEN

El presente trabajo tiene como objetivo la evaluación de las características aerodinámicas de sustentación y resistencia del Avión No Tripulado de Conservación Ecológica, por medio de ensayos en el túnel de viento y usando dinámica de fluidos computacional lineal combinada con un método analítico-empírico-numérico, para determinar la resistencia por fricción. Dos versiones del avión fueron evaluadas experimental y numéricamente. Las pruebas experimentales fueron llevadas a cabo en un túnel de viento no presurizado, de ciclo cerrado y sección cerrada Rollab SWT-009. Cada modelo fue construido a una escala de 1:21,6125. Fue creado un código capaz de estimar la resistencia de fricción de un aeroplano, el cual usa como datos de entrada la información de salida del código de alto orden PAN AIR. El código calcula el número de Reynolds local en el punto de control de cada panel, y luego la resistencia de fricción de cada uno de estos. La suma de la contribución de fricción de cada panel resulta en el coeficiente de resistencia por fricción. Los resultados experimentales para los diferentes números de Reynolds muestran una tendencia similar que a la obtenida en estudios previos con la misma aeronave. Los valores obtenidos por medio de la predicción numérica usados para estimar la resistencia viscosa concuerdan muy bien con los resultados experimentales para el número de Reynolds bajo condiciones de vuelo.

Palabras clave: predicción de resistencia aerodinámica, ensayos de túnel de viento, método de los paneles, dinámica de fluidos computacional lineal, aerodinámica

AERODYNAMIC CHARACTERISTICS OF AN UNMANNED AIRPLANE VIA WIND TUNNEL TESTING AND NUMERICAL ANALYSIS

ABSTRACT

The aim of this work is to evaluate the aerodynamic characteristics of lift and drag of the Unmanned Airplane for Ecological Conservation by using wind tunnel testing and using a linear computational fluid dynamic method combined with an analytical-empirical numerical method to determine skin-friction. Two versions of the airplane were evaluated experimentally and numerically. Experimental tests were carried out in an unpressurised, close-throat, and close circuit wind tunnel Rollab SWT-009. Each model was built on a 1:21.6125 scale. A code capable of estimating the skin-friction drag of the surface of an airplane was developed which uses output data from the high-order panel code PAN AIR as input. The code calculates the local Reynolds number in the control point of each panel, and then the skin-friction coefficient of each panel. The total skin-friction contribution of each panel results in the skin-friction drag coefficient. The experimental results at different Reynolds numbers show similar trends to those observed in previous studies with the same airplane. The values of drag coefficient agree with the experimental results at flight Reynolds number.

Keywords: aerodynamic drag prediction, wind tunnel testing, panel method, linear computational fluid dynamic, aerodynamics

NOMENCLATURE

A	=	panel area
C_L	=	lift coefficient
C_{Lmax}	=	maximum lift coefficient
C_{Lo}	=	lift coefficient at zero angle of attack
$C_{L\alpha}$	=	lift curve slope
C_D	=	drag coefficient
C_{Df}	=	skin-friction drag coefficient
C_{Di}	=	induced drag coefficient
C_{Do}	=	minimum drag coefficient
C_f	=	skin-friction coefficient
k	=	induced drag factor
l_x	=	distance for local Reynolds number
M	=	Mach number
Re	=	Reynolds number
Re_x	=	local Reynolds number
S	=	wing surface
V_t	=	tangential component of velocity on upper surface of the panel
$(L/D)_{max}$	=	maximum lift-drag ratio
ρ	=	air density
μ	=	dynamic viscosity
φ	=	velocity potential

INTRODUCTION

The Unmanned Airplane for Ecological Conservation (ANCE, Aeronave No tripulada de Conservación Ecológica) was designed to scout oil fields looking for oil spills to prevent or minimize ecological impact. The ANCE (figure 1) is a twin-boom, pusher-propeller unmanned airplane with a 5.187 m wingspan, a 3.1329 m^2 wing surface, an aspect ratio of 8.57, and a maximum takeoff mass of 182.055 kg (Cárdenas *et al.*, 2005). Early wind tunnel tests (Cárdenas *et al.*, 2005; Boschetti *et al.*, 2006) and linear non-viscous fluid dynamic analyses (Boschetti *et al.*, 2009; 2012) have been applied to study the aerodynamic performance of the vehicle. Advanced non-linear viscous fluid dynamic codes enable accurate aerodynamic analysis; nonetheless, these require substantial computer hardware and it is extremely time demanding. For these reasons, advanced computational fluid dynamic codes are not useful to evaluate viscous drag of the ANCE in the current phase of design. The drag coefficient is a very important parameter in design, performance estimation, and stability and control of airplanes.

Ahuja *et al.* (2010) created a code to predict the aerodynamic loads and distributions over a given airframe previously paneled on the surface. The code estimates the viscous drag coefficient by obtaining skin-friction drag using potential flow solution previously calculated via vortex-ring scheme. The code estimated of the viscous drag coefficient for a wide variety of airplanes has shown excellent results.

In this case, a code capable to estimate skin-friction drag was developed. The code uses output data from the code PAN AIR (Saaris, 1992) as input data. PAN AIR has been previously used to evaluate lift and induced drag coefficients of the ANCE (Boschetti *et al.*, 2009; 2012).

Additionally, wind tunnel experiments were carried out to evaluate the aerodynamic performance of the vehicle, and to validate numerical data obtained with PAN AIR and the prediction method used to calculate the skin-friction drag coefficient.

Two versions of the ANCE were experimentally and numerically evaluated. The original (ANCE X-2), and the modified version (ANCE X-3), which has a twisted area over the wing by flapping up the wing section. Figures 1 and 2 show the blueprints of the two versions of the ANCE. Figure 3 illustrates the twisted area over the wing in the modified version.

The main purpose of this work is to determine the aerodynamic characteristics of lift and drag coefficients, of the Unmanned Airplane for Ecological Conservation using wind tunnel testing, linear computational fluid dynamic method, and an analytical-empirical-numerical method to estimate skin-friction.

COMPUTATIONAL METHOD APPROACH

PAN AIR is a high order panel method computer program that is capable of solving a variety of boundary value problems in steady subsonic or supersonic inviscid and compressible flow. This can analyze the flowfield around a detailed and a complex three–dimensional geometry configuration (Epton and Magnus, 1990). The solutions are governed by the classical Prandtl-Glauert equation (Epton and Magnus, 1990; Tinoco *et al.*, 1980):

$$(1 - M^2)\phi_{xx} + \phi_{yy} + \phi_{zz} = 0 \qquad (1)$$

The surface geometry is divided up into networks, and these are subsequently divided into panels, wherein each panel

represents a linear source or a quadratic double singularity. The appropriate boundary condition equations are used to calculate the singularity strength parameters, which are used to compute the potential and velocity fields. Then, using an appropriate pressure–velocity relationship the pressure field can be calculated, and forces and moments can be computed by pressure integration (Epton and Magnus, 1990; Tinoco *et al.*, 1980; Derbyshire and Sidwell, 1982). The version A502i can perform a Trefftz Plane Analysis to calculate the induced drag of the vehicle, in order to correct the inaccuracies given by the calculation of the forces from the integration of pressure on the surface (Saaris, 1992, Katz and Plotkin, 2001).

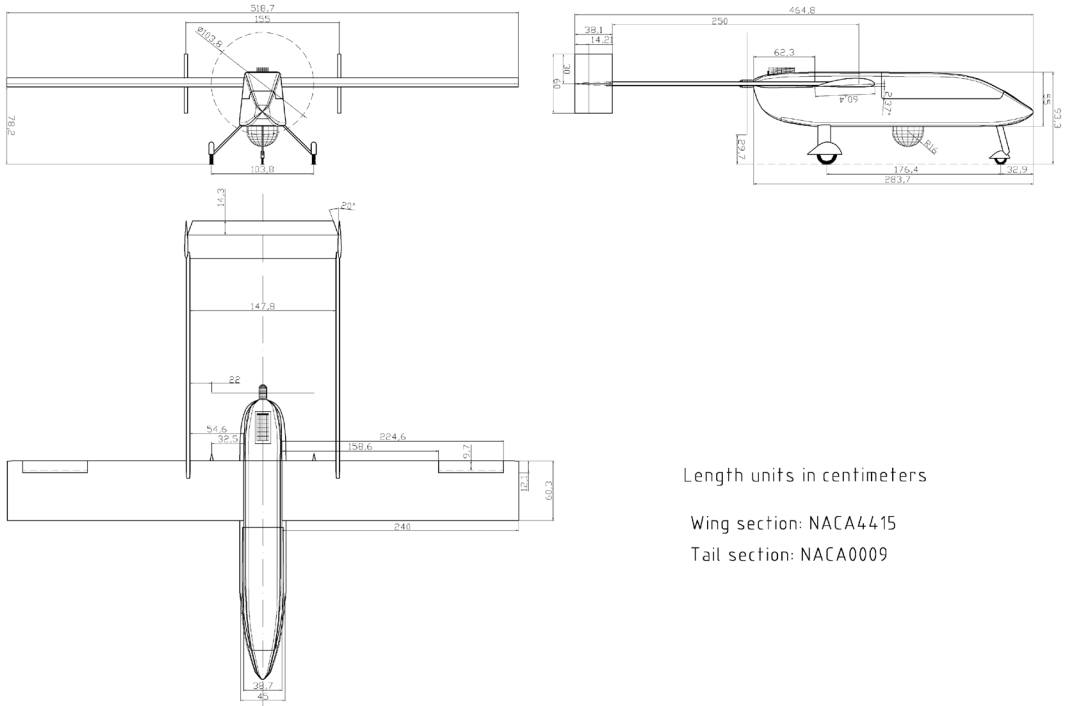

Figure 1. *Unmanned Airplane for Ecological Conservation, ANCE X-2*

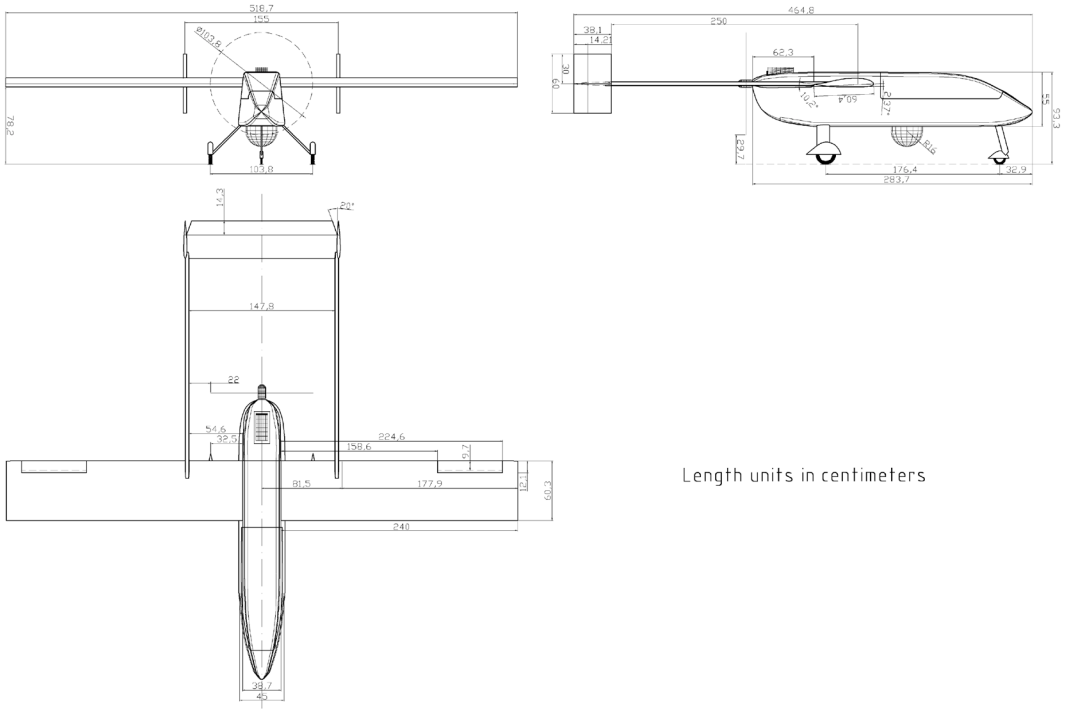

Figure 2. *Modified Unmanned Airplane for Ecological Conservation, ANCE X-3*

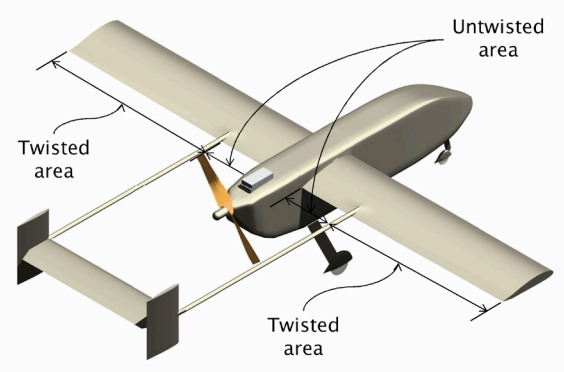

Figure 3. *Axonometric view of the modified airplane*

A program able to calculate the skin-friction drag coefficient of an airplane was written in MATLAB® (2009), which uses the output data from PAN AIR as input data. For each panel of the geometry, PAN AIR output data gives the coordinates of the control point, the upper surface unit normal vector scaled by ratio of panel area to reference area, and the tangential component of velocity on the upper surface, among others (Saaris, 1992). Using these values, the code calculates the local Reynolds number in each control point of the panel, using the equation:

$$Re_x = V_t \cdot l_x \cdot \rho / \mu \qquad (2)$$

where the path length between the leading edge (for lifting surfaces) or the nose (for fuselage bodies) and the control point is l_x, and the tangential component of velocity on upper surface of the panel is V_t. Based on the local Reynolds number in a panel, the flow could be laminar for $Re_x \leq 5\times10^5$, turbulent for $Re_x \geq 1\times10^6$, or in transition for $5\times10^5 < Re_x < 1\times10^6$.

For very low Reynolds numbers, $Re_x \leq 1$, Eq. (3) is used to estimate the local skin-friction coefficient (Hoerner, 1965).

$$C_f = 10.9 / \left[Re_x \left(1.4 - logRe_x \right) \right] \qquad (3)$$

Equation (4) is an analytical expression used to estimate the local skin-friction coefficient in laminar flow ($1 < Re_x \leq 5\times10^5$) (Incropera and DeWitt, 1990).

$$C_f = 0.664 / \sqrt{Re_x} \qquad (4)$$

Schlichting (1973) derived an empirical equation to calculate the local skin-friction coefficient in turbulent flow,

$$C_f = 0.0592 / Re_x^{1/5} \qquad (5)$$

In transition flow, Eq. (6) is used (Hoerner, 1965).

$$C_f = 0.0592 / Re_x^{1/5} - 1700 / Re_x \qquad (6)$$

Equation (7) is used to estimate the drag coefficient of a configuration without considering boundary layer separation, if the values of skin-friction coefficient of each panel are known.

$$C_{Df} = \frac{1}{S} \sum_{i=1}^{n} \left(A_i \cdot C_{fi} \right) \qquad (7)$$

LINEAR COMPUTATIONAL FLUID DYNAMIC ANALYSIS AND VISCOUS DRAG ESTIMATION

The flowfield around the two versions of the airplane was analyzed using the three-dimensional panel code PAN AIR, version 502i (Saaris, 1992). Figures 4 and 5 show the surface paneling of the airplane simulated with PAN AIR. Each half-configuration consists of 3,009 panels and twenty-seven surface networks. Twenty-two surface networks defined as indirect condition on impermeable thick surface modeled the lifting surfaces, four surface networks defined as direct condition on impermeable thick surface modeled the non-lifting surfaces, and one surface network was defined as base surface condition. Seventeen wake surfaces networks were necessary to satisfy the Kutta condition (zero vorticity at trailing-edges and body bases), and each having twenty-five chord lengths. Grid sensitivity studies demonstrated very little dependency of the aerodynamic coefficients. Similar paneled geometries were previously tested by (Boschetti *et al.*, 2012).

The paneled geometries were analyzed at different angles of attack in steady flow at Mach 0.15 (Boschetti *et al.*, 2012). Lift coefficient was computed by pressure integration, and induced drag coefficient was calculated by the Trefftz Plane Analysis.

Some components of the airplane as the camera, the landing gear, and the engine were not included in the analyzed configuration with PAN AIR, because the flow separation has a strong influence on the drag generated by these components. Besides, forces and moments produced by these components could be considered insignificant in inviscid flow.

Figure 4. *Paneled half-geometry and wakes simulated by PAN AIR. The wakes are downstream of the airplane geometry*

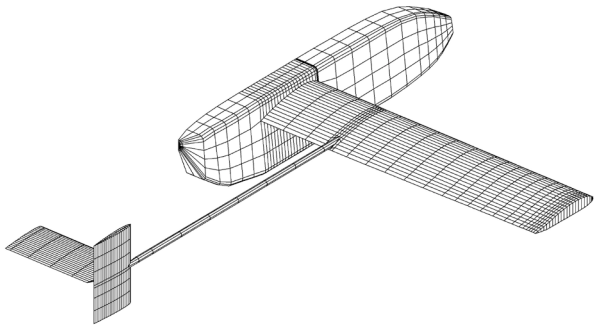

Figure 5. *Surface paneling of the airplane*

For each angle of attack, the output data given by PAN AIR were utilized to estimate the drag coefficient using the code wrote with MATLAB®. The drag generated by the components not included in the paneled geometry was estimated by analytical-empirical methods. The drag coefficient of the camera and the engine were obtained using the empirical approximations shown by Hoerner (1965) and Mises (1959). The drag coefficients of the landing gears were calculated using the data presented by Torenbeek (1976).

WIND TUNNEL EXPERIMENTS

Experimental tests were carried out in a Rollab SWT-009 wind tunnel located in the facilities of the Department of Aeronautical Engineering of the National Experimental Polytechnic University of the Armed Forces (UNEFA), Maracay, Venezuela, between March and June 2011. This wind tunnel is an unpressurised, close-throat, and close

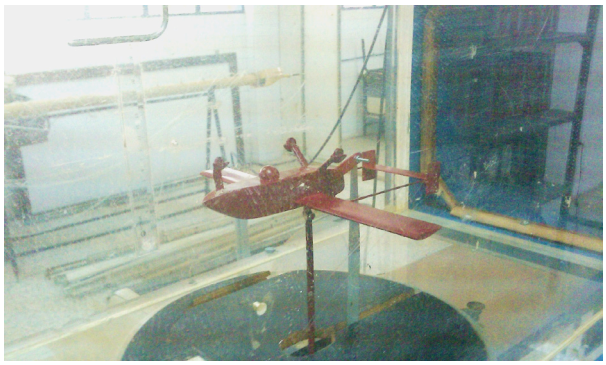

Figure 6. *Original airplane (ANCE X-2) model inside the test section in inverted position*

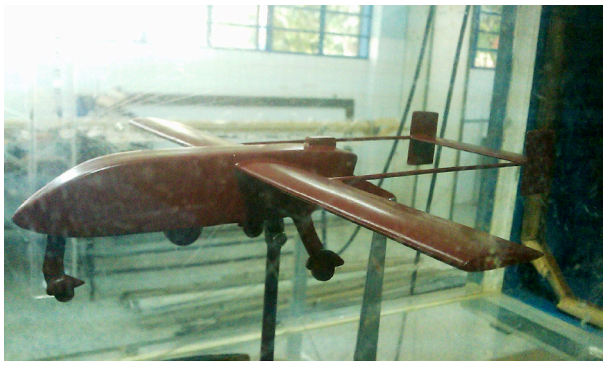

Figure 7. *Modified airplane (ANCE X-3) model in the wind tunnel*

circuit wind tunnel, with a maximum airspeed of about 50 m/s. It is used to test wings and small three-dimensional models mainly for academic and research projects. The tunnel has a close, transparent, square test section of 0.30 m×0.30 m, and it uses a three-component balance (lift, drag and pitching moment) to measure lift and drag forces, and pitching moment. The balance can support the models by three or two struts. The airflow speed can be determined by means of the pressure differences between the test section and the downwash section and/or using a pitot tube.

The wind tunnel models of the airplanes have a wingspan of 0.24 m and a wing surface of 67.0723 cm^2 (scale 1:21.6125), a wingspan equal to 80% of the test section. These models were made with acrylonitrile-butadiene-styrene by a rapid prototyping machine using fused deposition modeling. The internal wing structure was reinforced with steel beams of 3/32 in (0.238125 cm), and the wing booms were fabricated using steel beams of 1/16 in (0.15875 cm). Each part was smoothed, and then assembled and glued with cyanoacrylate. Finally, both models were painted in red and covered with sealant. Figures 6 and 7 show the original and modified airplane models, respectively, inside of the test section.

The three-component balance system of the wind tunnel was calibrated for lift and drag forces using a smooth sphere with a diameter of 6.4 cm, and a single wing of the same wingspan, aspect ratio and airfoil section of the original airplane test model. Both sphere and wing were tested at different airspeeds to achieve forces at different test Reynolds numbers. The results obtained for the sphere were compared with experimental data presented by Hoerner (1965). The force values of the single wing were compared against analytical Prandtl's lifting line theory and experimental data for airfoil NACA4415 (Jacobs and Sherman, 1936). Additionally, the turbulence factor of the wind tunnel was 16. It was calculated using the sphere and the single wing.

Both airplane models were tested in normal and inverted position to correct the balance aerodynamic alignment, the sting and support tare and the interference. Wind tunnel wall effects and blockage were considered using the techniques described by Rae and Pope (1984).

A more detailed review of the wind tunnel tests procedure can be found in Mujica and Vera (2011).

RESULTS AND DISCUSSION

Wind tunnel experiments

The wind tunnel experiments were carried out at several Reynolds numbers in order to study the behavior of the test models as a function of Reynolds number.

Figure 8 shows that induced drag factor of both models decreases while the Reynolds number increases. According to lifting line theory, the induced drag factor is independent of Reynolds number at high *Re*. In this case, the viscous effects are considerable and affect *k* at these *Re*. Figure 9 shows that the curve of minimum drag coefficient as a function of Reynolds number have a similar trend to the one reported by Jacobs and Sherman (1936). It could be observed that the minimum drag coefficient curve falls as the Reynolds number increases until it reaches $Re=4.32\times10^5$, then this has a slight increase, and finally, a negative slope. This behavior represents the transition from laminar to turbulent flow regime. Similar observations were done by Cárdenas *et al.* (2005) and Boschetti *et al.* (2006) for the ANCE X-2. Figure 10 shows how the lift coefficients at zero angle of attack of both models change considerable with *Re*, due to flow regime transition. Furthermore, figure 11 shows similar trend reported by Jacobs and Sherman (1936) for lift curve slope. However, the maximum lift coefficient curves presented in figure 12 do not match with the trend presented by Jacobs and Sherman (1936). Maximum lift coefficient should increase while *Re* increases.

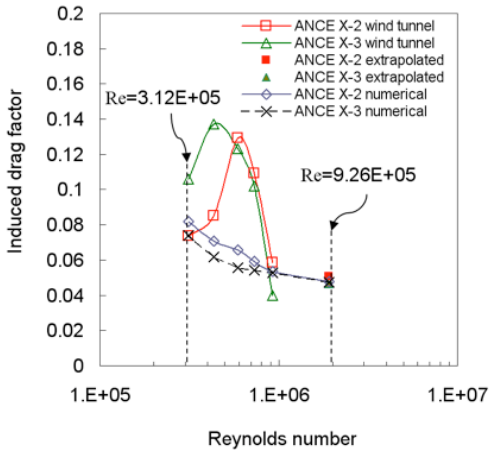

Figure 8. *Induced drag factor as a function of Reynolds number*

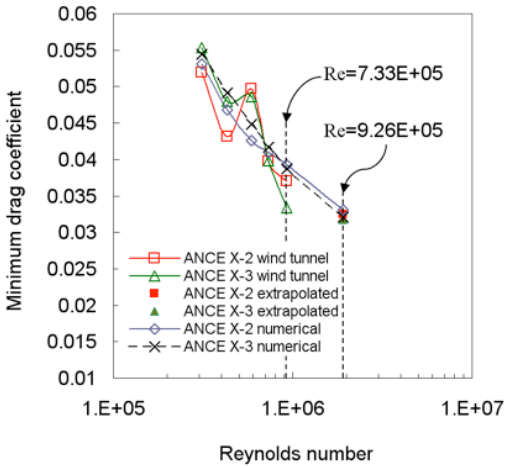

Figure 9. *Minimum drag coefficient as a function of Reynolds number*

Errors measuring C_{Lmax} of the models could occur due to false appreciation of stall at low Reynolds numbers.

The measuring errors achieved in lift and drag coefficients for high angles of attack were ±0.0018165 and ±0.0011736, respectively, and for low angles of attack were ±0.0001559 and ±0.0004895, respectively. Errors estimation is based in errors measurement of the balance, the manometers, and the thermometer.

Scaling to free flight condition

Because the wind tunnel tests were performed at Reynolds numbers different from the value at free flight condition, it is necessary to extrapolate the results to flight Reynolds number.

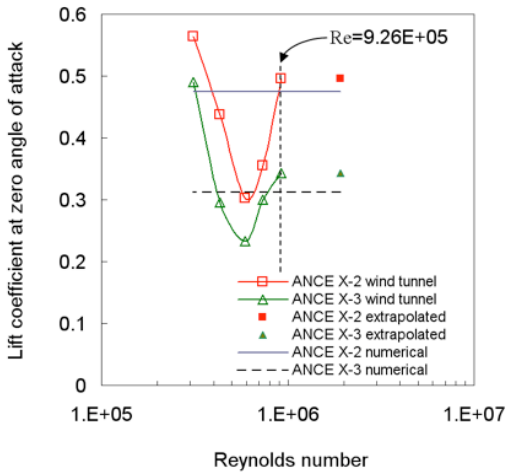

Figure 10. *Lift coefficient at zero angle of attack as a function of Reynolds number*

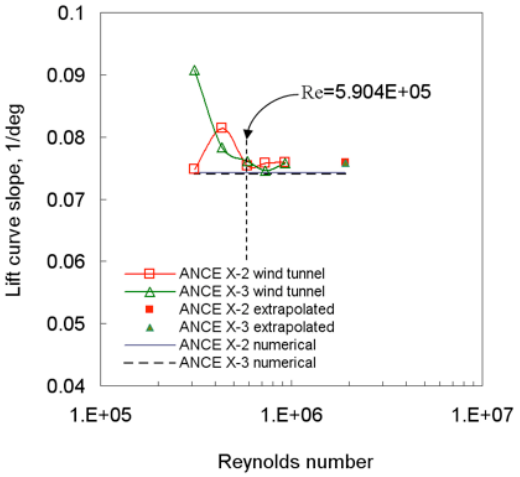

Figure 11. *Lift curve slope as a function of Reynolds number*

The Jacob's Method (Jacobs and Sherman, 1936) was used to estimate the maximum lift coefficient at flight Reynolds number (Re_{flight}) of the original (ANCE X-2) and modified (ANCE X-3) airplanes because the chord-based test Reynolds number (Re_{test}) value is smaller than Re_{flight} (Re_{test}=9.26×10^5, Re_{flight}=1.916×10^6). In this method, it is supposed that the lift slope and the lift coefficient at zero angle of attack are equal for both conditions and the maximum lift coefficient is extrapolated to free flight condition based on empirical data. This method can be easily applied in this case because the airplane wing section is a NACA4415.

The drag polar curve obtained in the wind tunnel for the two models was adjusted to flight Reynolds number using the second method of extrapolating explained by Pettersson and Rizzi (2008), which is based in the third extrapolating

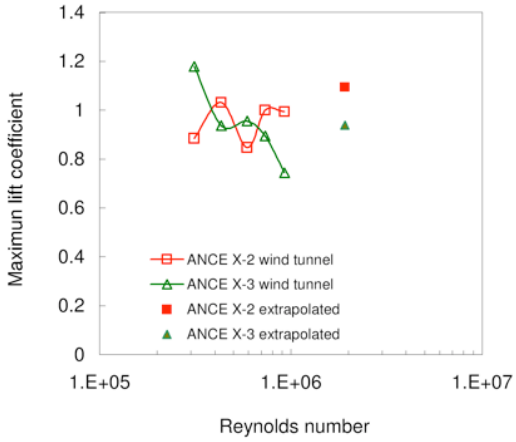

Figure 12. *Maximum lift coefficient as a function of Reynolds number*

method described by Rae and Pope (1984). Figures 13 and 14 show the extrapolation of lift-drag polar curve at flight Reynolds number for both airplane models. The viscous drag coefficient is extrapolated using the equation of Jacobs and Sherman (1936):

$$(C_D - C_{Di})_{flight} = (C_D - C_{Di})_{test} (Re_{test}/Re_{flight})^m \qquad (8)$$

The value of the exponent m is assumed equal to 0.11 after Jacobs and Sherman (1936) who found that this value is the best fit for airfoils sections.

Figures 15-20 show the aerodynamic data obtained at Re_{flight} in the wind tunnel. From the experimental values observed in these figures the minimum drag coefficient was obtained (Figures 15 and 16), the lift coefficient at zero angle of attack (Figures 17 and 18), the maximum lift coefficient (Figures 17 and 18), and the maximum lift-drag ratio (Figures 19 and 20). Additionally, the induced drag factor and lift curve slope were estimated. Table 1 presents the values obtained for both airplanes. The comparison between the aerodynamic characteristics of both versions of the airplane (ANCE X-2 and ANCE X-3) will be discussed later connected with the numerical results obtained with the proposed empirical-analytical-numerical method.

Figures 8-11 present a comparison of the numerical data and experimental results at various Reynolds numbers for both the ANCE X-2 and the ANCE X-3.

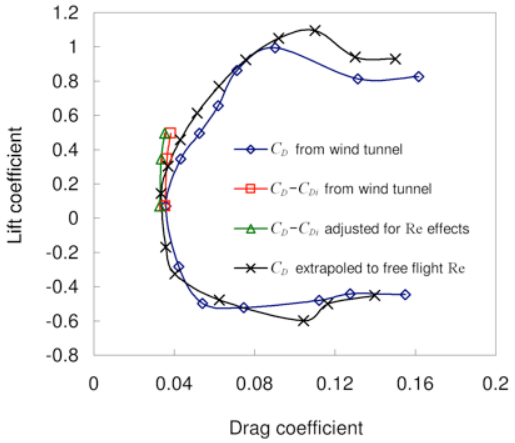

Figure 13. *Extrapolation of lift-drag polar of original airplane ANCE X-2*

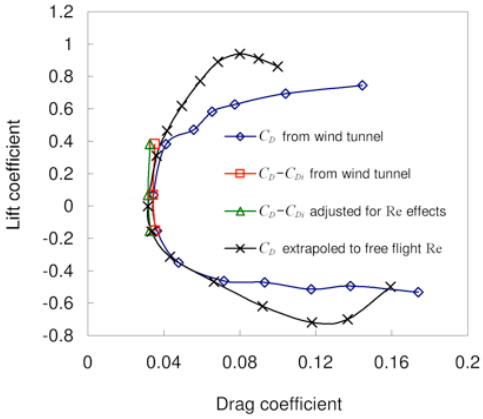

Figure 14. *Extrapolation of lift-drag polar of modified airplane ANCE X-3*

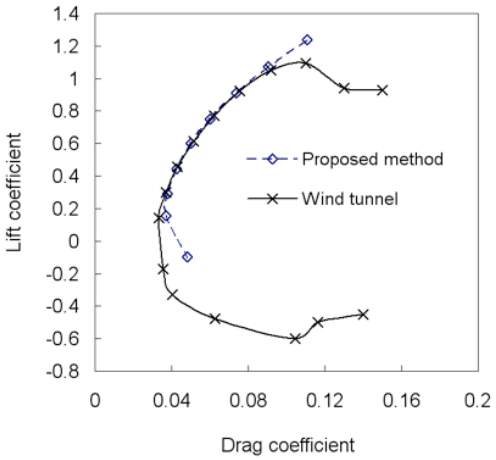

Figure 15. *Lift coefficient as a function of drag coefficient at flight Reynolds number of original airplane ANCE X-2*

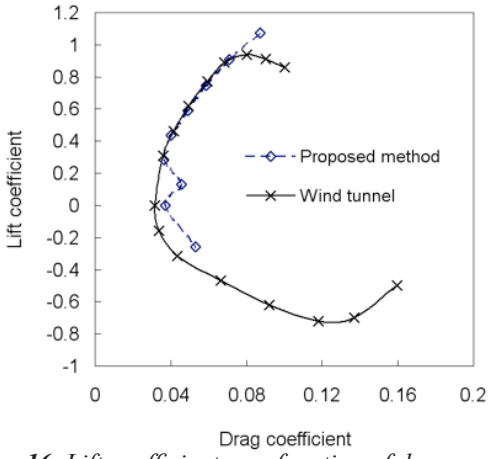

Figure 16. *Lift coefficient as a function of drag coefficient at flight Reynolds number of modified airplane ANCE X-3*

Figure 8 shows that the induced drag factor values calculated for the ANCE X-2 using the proposed empirical-analytical-numerical method have slightdifferences at Re=3.12×10^5 and Re=9.26×10^5, which correspond to laminar and high transition flow regimes, respectively. The results of these comparisons show in figure 9 that the minimum drag coefficient values achieved with the numerical-empirical method fit those obtained experimentally at Re=3.12×10^5, i.e. in the laminar flow regime. For the ANCE X-2, these closely fit at Reynolds number values equal to 7.33×10^5 and 9.26×10^5 corresponding to transition flow regime. The lift coefficient at zero angle of attack values presented in figure 10 accomplished by PAN AIR are close from those obtained experimentally at Re=9.26×10^5. Figure 11 shows that the lift curve slope values calculated by PAN AIR are slightly smaller than those measured from wind tunnel testing for Re≥5.904×10^5 corresponding to transition flow regime. Excluding these observations, the values obtained using the proposed prediction method in laminar and transition flow are substantially different from those obtained in the wind tunnel. The differences between the values of C_{Do} and k obtained using wind tunnel testing and the proposed method are due to the proposed method supposes that at low angles of attack, the boundary layer separation is negligible, and this could be a mistaken assumption at low Reynolds numbers, especially in transition flow regime. The values of $C_{L\alpha}$ and C_{Lo} were computed directly by PAN AIR (a potential flow code), and in low Reynolds number flows viscous effects are dominant, explain why the significant differences with respect to experimental values obtained at these Re.

Figures 15-20 show the data obtained using the proposed empirical-analytical-numerical method at flight Reynolds number. These data are obtained using the method proposed in this paper at Re_{flight}=1.916×10^6. The estimated data agree very well with the experimental results for both models when the flow separation phenomena are negligible. When predicted results are compared against experimental data, the induced drag factor values achieve a difference

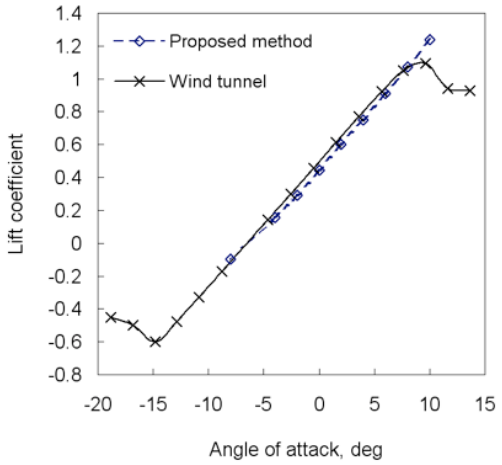

Figure 17. *Lift coefficient as a function of angle of attack at flight Reynolds number of original airplane ANCE X-2*

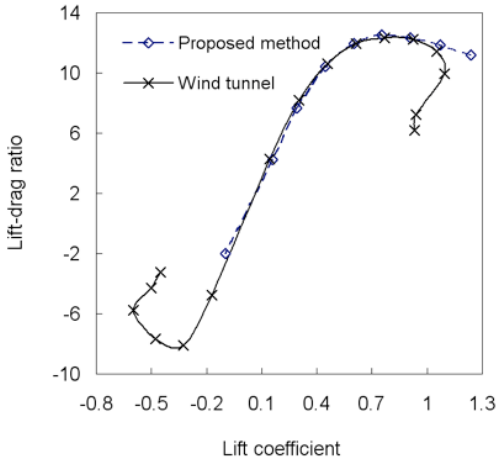

Figure 19. *Lift-drag ratio as a function of lift coefficient at flight Reynolds number of original airplane ANCE X-2*

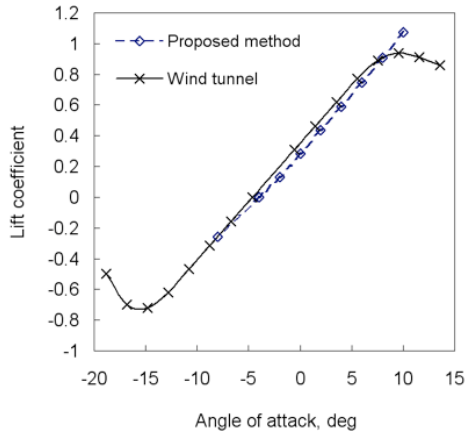

Figure 18. *Lift coefficient as a function of angle of attack at flight Reynolds number of modified airplane ANCE X-3*

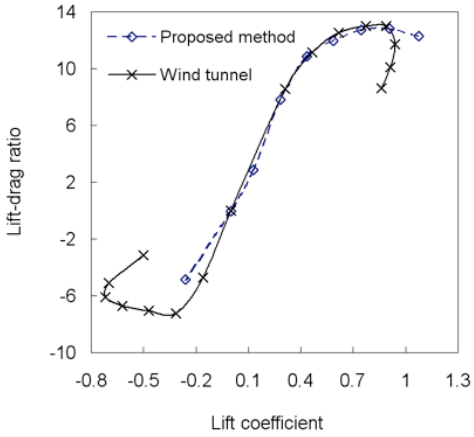

Figure 20. *Lift-drag ratio as a function of lift coefficient at flight Reynolds number of modified airplane ANCE X-3*

of 5.743% and 1.940% for the original (ANCE X-2) and the modified version (ANCE X-3), respectively. For the minimum viscous drag coefficient values the difference is 2.160% and 1.262%, respectively; the lift slope values achieve a maximum difference of 2.375%, while the lift coefficient at zero angle of attack values reach 4.297% and 8.762% for the original and modified models, respectively.

Table 1 shows that the addition of twist to the aircraft wing reduces the induced drag factor, the minimum drag coefficient, the lift coefficient at zero angle of attack, and the maximum lift coefficient, and produces slight changes in the lift slope compared to the original airplane. The induced drag factor obtained by wind tunnel testing and using the proposed method diminishes 8.119% and 0.630%, respectively, and the minimum viscous drag

Table 1. Aerodynamic data at flight Reynolds number

	k	C_{Do}	$(L/D)_{max}$	C_{La}, 1/deg	C_{Lo}	C_{Lmax}
Original airplane, ANCE X-2						
Wind tunnel test	0.0505	0.0324	12.361	0.0759	0.4957	1.094
Prediction method	0.0476	0.0331	12.597	0.0742	0.4744	-
Modified airplane, ANCE X-3						
Wind tunnel test	0.0464	0.0317	13.037	0.0758	0.3424	0.9389
Prediction method	0.0473	0.0321	12.832	0.0740	0.3124	-

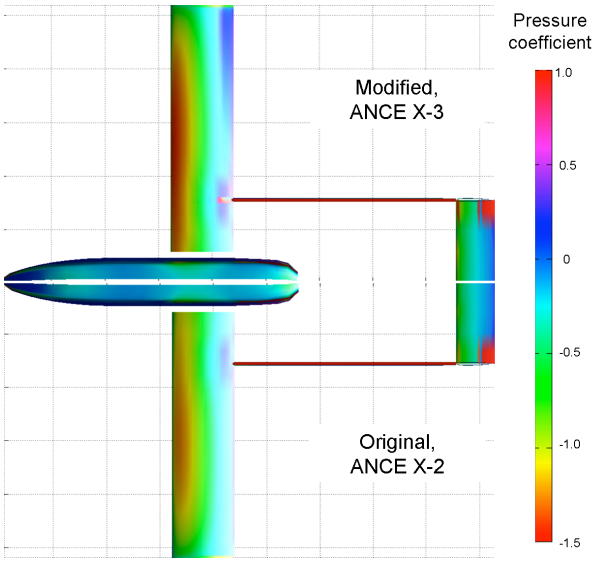

Figure 21. *Pressure coefficient distribution on the airplane. Bottom is shown ANCE X-2 and top ANCE X-3*

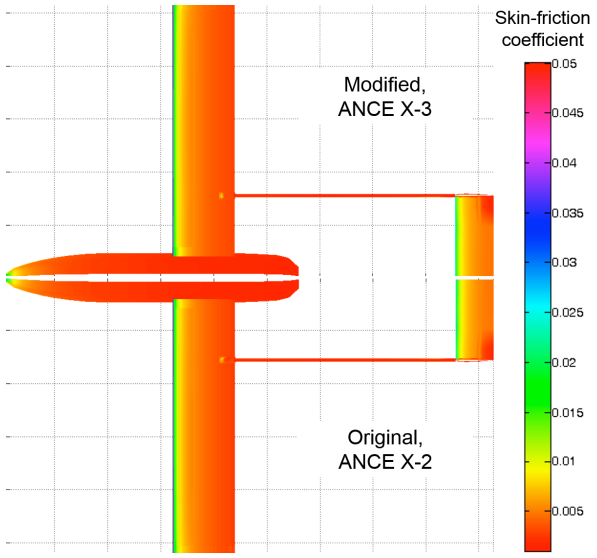

Figure 22. *Skin-friction coefficient distribution on the airplane. Bottom is shown ANCE X-2 and top ANCE X-3*

coefficient obtained by both methods reduces 2.16% and 3.021%, respectively. Moreover, the addition of wing twist increases the maximum lift-drag ratio 5.47% and 1.867%, experimentally and using the present prediction method, respectively. The decrease of induced drag factor and the reduction in viscous drag cause the increase of maximum lift-drag ratio. The increase of maximum lift-drag ratio obtained using wind tunnel testing represents an improvement of the performance characteristic of the airplane in cruise flight. Although the proposed method does not predict accurately the difference between the values of k, C_{Do} and $(L/D)_{max}$ of the original (ANCE X-2) and the modified (ANCE X-3) airplanes, this predicts that the wing twist addition increases $(L/D)_{max}$, and reduces k and C_{Do} respect to the original airplane, quite useful in early phases of preliminary design. Furthermore, the wind tunnel experiments show a reduction of the maximum lift coefficient obtained for the modified airplane (ANCE X-3) of 14.177% compared to the original airplane (ANCE X-2), an expected change in performance when wing twist is applied to increase $(L/D)_{max}$. C_{Lmax} reduction would increase the stall speed, and it has to be investigated in future performance studies in order to guarantee safe flight. The results of inviscid force coefficients agree with the results reported by Boschetti *et al.* (2012).

Figures 21 and 22 show the pressure coefficient distribution and skin-friction coefficient distribution for both the ANCE X-2 and the ANCE X-3, at cruise lift coefficient, C_L=0.745 (Boschetti *et al.*, 2012). Figure 21 shows that the wing twist modification change the wing pressure coefficient distribution in order to reduce the washout (Boschetti *et al.*, 2012). Figure 22 presents that the skin-friction coefficient distribution is slightly different only next to the wing tip, which may be the cause of the reduction of minimum drag coefficient of the ANCE X-3 when compared to the ANCE X-2.

CONCLUSIONS

This paper focused on the determination of the aerodynamic characteristics of lift and drag of the Unmanned Airplane for Ecological Conservation using wind tunnel testing and numerical analysis. A prediction code to estimate skin-friction drag coefficient of an airplane was developed. The code uses the output from the high-order panel code PAN AIR as input data.

The viscous drag calculated using the code agreed very well with experimental results at flight Reynolds number. For lower values of Reynolds number (Re=3.12×10^5), only the minimum drag coefficient was satisfactory. For Re≥5.904×10^5, a comparison between the values of the non-viscous force coefficients computed by the code PAN AIR and the experimental values show that the lift curve slope values obtained using PAN AIR are slightly smaller than those measured through wind tunnel testing. For Re<9.26×10^5, the lift coefficient at zero angle of attack values calculated with the panel code are far removed from those measured in the wind tunnel. The proposed method calculates accurate approximations when the airplane is simulated in turbulent flow.

Experimental and numerical results show that the wing twist modification applied to the ANCE diminishes the induced drag factor and the minimum drag coefficient and increases the maximum lift-drag ratio.

The code can estimate skin-friction drag coefficient accurately for the Unmanned Airplane for Ecological Conservation at flight Reynolds numbers.

ACKNOWLEDGMENTS

The authors would like to thank the Department of Aeronautical Engineering of National Experimental Polytechnic University of the Armed Forces (UNEFA) in Maracay, Venezuela, for allowing us to use the wind tunnel facilities. The authors acknowledge the financial support of Decanato de Investigación y Desarrollo (DID) of Univesidad Simón Bolivar in Caracas, Venezuela. P. J. B. and E. M. C. authors thank the reviewers due to their comments and suggestions which helped us to improve the quality of this article.

REFERENCES

Ahuja, V., Burkhalter, J., & Hartfield, R. (2010, January) Preliminary Design Drag Calculation Using Advanced Paneling Schemes (Paper No. AIAA-2010-0063). In the proceedings of 48th AIAA Aerospace Sciences Meeting and Exhibit, Orlando, Florida.

Boschetti, P., Cárdenas, E., & Amerio, A. (2006). Drag Clean-up Process of the Unmanned Airplane for Ecological Conservation. Aerotecnica Missili e Spazio, 85(2), 53-62.

Boschetti, P. J., Cárdenas, E. M., & Amerio, A. (2009, January). Aerodynamic Analysis of the Unmanned Aerial Vehicle for Ecological Conservation (Paper No. AIAA-2009-1480). In the proceedings of 47th AIAA Aerospace Sciences Meeting and Exhibit, Orlando, Florida.

Boschetti, P. J., Cárdenas, E. M. & Amerio, A. (2012, January). Induced Drag Reduction of an Airplane using Local Twist, Panel Method Verification (Paper No. AIAA-2012-0267). In the proceedings of 50th AIAA Aerospace Sciences Meeting including the New Horizons Forum and Aerospace Exposition, Nashville, Tennessee.

Cárdenas, E., Boschetti, P., Amerio, A., & Velásquez, C. (2005, September). Design of an Unmanned Aerial Vehicle for Ecological Conservation (Paper No. AIAA-2005-7056). In the proceedings of Infotech@Aerospace, Arlington, Virginia.

Derbyshire T. & Sidwell K. W. (1982). PAN AIR Summary Document (Version 1.0), NASA CR-3250. Washington D.C: National Aerospace and Space Administration.

Epton, M. A. & Magnus, A. E. (1990). PAN AIR: A Computer Program for Predicting Subsonic or Supersonic Linear Potential Flows About Arbitrary Configurations Using A Higher Order Panel Method, Vol. 1. Theory Document (Version 3.0), NASA CR-3251. (revision 1). Washington D.C: National Aerospace and Space Administration.

Hoerner, S. F. (1965). Fluid-Dynamic Drag, New York City: Published by the Author.

Incropera, F. P., & Dewitt, D. P. (1990). Fundamentals of Heat and Mass Transfer, 3rd ed. New York City: John Wiley & Sons.

Jacobs, E. N., & Sherman, A. (1936). Airfoil Section Characteristics as Affected by Variations of the Reynolds Number, NACA R-586. Washington D.C: National Advisor Committee for Aeronautics.

Katz, J., & Plotkin, A. (2001). Low-Speed Aerodynamics, 2nd ed. New York City: Cambridge University Press.

MATLAB (2009). The MathWorks, Inc., Software Package, Ver. 7.8.0 (R2009a). Natick, MA.

Mises (Von), R. (1959). Theory of Flight. New York City: Dover Publications.

Mujica, L. & Vera, G. (2011). Evaluación Aerodinámica Experimental del Avión No Tripulado De Conservación Ecológica, ANCE X-3d. Engineering Thesis. Caracas, Venezuela: Universidad Nacional Experimental Politécnica de la Fuerza Armada.

Pettersson, K. & Rizzi, A. (2008). Aerodynamic Scaling to Free Flight Conditions: Past and Present, Progress in Aerospace Sciences, 44 (4), 295-313. doi:10.1016/j.paerosci.2008.03.002

Rae, W. H., & Pope, A. (1984). Low-Speed Wind Tunnel Testing, 2nd ed. New York City: Wiley Interscience Publication.

Saaris, G. R. (1992). A501i User's Manual - PAN AIR Technology Program for Solving Problems of Potential

Flow about Arbitrary Configurations, Report D6-54703. Seattle, Washington: The Boeing Company.

Schlichting, H. (1973). Boundary layer Theory, 6th ed. New York City: McGraw-Hill.

Tinoco, E. N., Johnson, F. T., & Freeman, L. M. (1980). Application of a Higher Order Panel Method to Realistic Supersonic Configurations, Journal of Aircraft, 17 (1), 38–44. doi: 10.2514/3.44647

Torenbeek, E. (1976). Synthesis of subsonic airplanes design. Rotterdam, The Netherlands: Delft University Press.